Chaotic advection and relative dispersion in an experimental convective flow

G. Boffetta[a)]
Dipartimento di Fisica Generale, Università di Torino Via Pietro Giuria 1, 10125 Torino, Italy

M. Cencini[b)]
Dipartimento di Fisica, Università di Roma ''la Sapienza,'' Piazzale Aldo Moro 5, 00185 Roma, Italy

S. Espa
Dipartimento di Idraulica Trasporti e Strade, Università di Roma ''la Sapienza,'' Via Eudossiana 18, I-00184 Roma, Italy

G. Querzoli
Dipartimento di Ingegneria del Territorio, Universitá di Cagliari, P.zza d'Armi, I-90123, Cagliari, Italy

(Received 30 November 1999; accepted 14 August 2000)

Lagrangian motion in a quasi-two-dimensional, time-dependent, convective flow is studied at different Rayleigh numbers. The particle tracking velocimetry technique is used to reconstruct Lagrangian trajectories of passive tracers. Dispersion properties are investigated by means of the recently introduced finite size Lyapunov exponent analysis. Lagrangian motion is found to be chaotic with a Lyapunov exponent which depends on the Rayleigh number as $\mathrm{Ra}^{1/2}$. The power law scaling is explained in terms of a dimensional analysis on the equation of motion. A comparative study shows that the fixed scale method makes more physical sense than the traditional way of looking at the relative dispersion at fixed times. © *2000 American Institute of Physics.* [S1070-6631(00)00112-4]

I. INTRODUCTION

The understanding of transport and mixing properties of passive impurities in fluid flows is of great practical importance in several fields of earth sciences and engineering.[1] In spite of its relevance, a general theory for the dynamics of passive impurities in a given flow is still lacking due to the well-known difficulties in connecting Eulerian and Lagrangian statistics.[2]

Traditionally, the study of passive transport can be divided into two broad classes: transport in laminar and in turbulent flows. Usually, the transition between the two different flow regimes can occur by changing some control parameters, e.g., Rayleigh number Ra in convective flows. At small Ra the fluid is motionless and the transport is entirely due to molecular diffusion. In the limit of very large Ra turbulence is completely developed and diffusive properties can be phenomenologically described by the introduction of an ''eddy'' diffusion coefficient.[3]

In this paper we are interested in an intermediate regime in which we observe a two-dimensional, almost time-periodic Eulerian flow. In this regime it is now well known that the Lagrangian motion of passive particles can be very complex due to chaotic advection,[4–6] see also Refs. 7–9. The equations of motion for a fluid particle in two-dimensional, incompressible, time-dependent flows formally constitute a nonautonomous one degree of freedom Hamiltonian system, where the stream function plays the role of the Hamiltonian. As a consequence, particle trajectories can display Hamiltonian chaos[10] and, therefore, strong sensitivity to initial conditions. The interest in studying the chaotic properties of Lagrangian trajectories is in the characterization of the mixing properties of the passive particles.[5,6,8,11]

Previous experimental studies of chaotic advection in convective flows have limited the parameter variability to a small range in order to keep the flow two dimensional.[7] In the present work we use a configuration in which the fluid motion is forced to be essentially two-dimensional (see Ref. 12). The convection is generated in a rectangular tank by a linear heat source positioned in the symmetry plane of the bottom surface of it. In this configuration, the Eulerian features of the flow are controlled by three nondimensional parameters:[13] the Rayleigh number $\mathrm{Ra}=(g\beta QH^3)/(\alpha\nu\kappa)$, the Prandtl number $\mathrm{Pr}=\nu/\kappa$, and the aspect ratio $A=H/L$, where g is the gravitational acceleration, β the thermal expansion coefficient of the fluid, α the thermal conductivity, ν the kinematic viscosity, κ the thermal diffusivity, Q the heat flux per unit length of the linear source, H the height of the tank, and L its width. In the range of the parameters of our experiments the flow consists of two main counter-rotating rolls divided by an ascending thermal plume above the heat source.[14] The upper end of the plume oscillates horizontally almost periodically with a frequency depending on the Rayleigh number.

Lagrangian trajectories are identified on a vertical plane by the particle tracking velocimetry technique (PTV).[15] Chaotic features of the Lagrangian motion are directly investigated by looking at the separation growth of initially close

[a)]Also at: Istituto Nazionale Fisica della Materia, Unità di Torino.
[b)]Also at: Istituto Nazionale Fisica della Materia, Unità di Roma.

 © 2000 American Institute of Physics

Downloaded 17 May 2001 to 192.167.149.117. Redistribution subject to AIP license or copyright, see http://ojps.aip.org/phf/phfcr.jsp

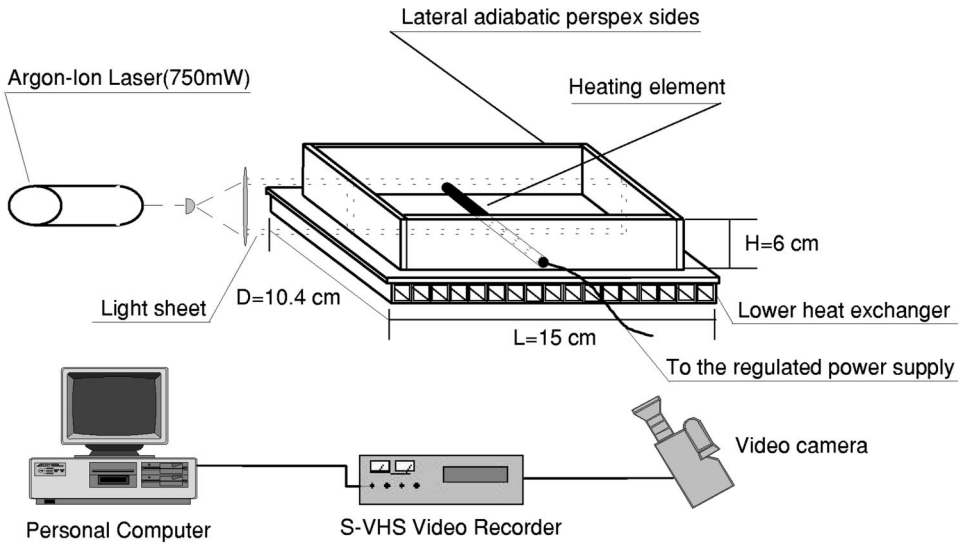

FIG. 1. Experimental setup. The upper cooling system (not shown) is similar to the lower one.

trajectories. In particular, we compute the finite size Lyapunov exponent (FSLE) recently introduced in Ref. 16. This indicator gives a characterization of the spreading mechanisms acting on different length scales recovering at small scales the Lagrangian Lyapunov exponent.[17] In order to explore possible links between Eulerian and Lagrangian properties, we also study the dependence of the Lagrangian statistics on the Rayleigh number.

The paper is organized as follows. Section II describes the experimental setup and the measuring technique. In Sec. III we summarize the finite size Lyapunov exponent analysis. Section IV presents the experimental evaluation of the FSLE and the dependence on the Rayleigh number. Section V contains some conclusions. In the Appendix we produce some detail on the finite size Lyapunov exponent analysis.

II. EXPERIMENTAL SETUP AND MEASURING TECHNIQUE

The experiment is performed in the rectangular tank filled with water sketched in Fig. 1. The tank is $L=15.0$ cm wide, 10.4 cm deep, and $H=6.0$ cm height. The upper and lower surfaces are 0.8 cm thick made of aluminum plates, kept at a constant temperature by means of two counterflow heat exchangers consisting of square-shaped pipes where water flows at constant temperature. The side walls are made of 1.0-cm-thick perspex and can be considered adiabatic.

The convection is generated by a linear heat source, a circular cylinder 0.8 cm in diameter, located in the midline of the tank 0.4 cm above the lower surface. The cylinder is heated by an internal electrical resistance connected to a stabilized power supply that controls the heat flux furnished to the system with a precision of 2%. The mean temperature of the fluid is probed by a thermocouple in order to evaluate its global physical properties, such as kinematic viscosity, thermal diffusivity, and thermal expansion coefficient.

Lagrangian description of the fluid motion is carried out by means of the PTV technique. To this aim, the fluid is seeded with a large number of small (50 μm in diameter), neutrally-buoyant pine pollen particles. The vertical plane, in the middle of the tank and orthogonal to the heat source, is illuminated by a 0.3-cm-thick light sheet generated by a 750 mW argon-ion laser through a cylindrical lens. A standard charge coupled device video camera, orthogonal to the light sheet, takes a series of single-exposure images of the test section. The images are recorded on a S-VHS tape and digitized at a 8.33 Hz rate with a 752×576 pixel resolution.

The PTV technique allows us to detect, position, and track individual particle images over a set of the acquired frames and thus to reconstruct a continuous velocity field from the sparse vectors. The procedure used to detect particle locations over the digitized frame consists of three steps. First, the digitized frames are segmented by means of a threshold operator that discerns pixels belonging to the particle images or to the background: The image is reduced to a Boolean representation in which the nonzero values identify the particle images whereas the null ones are associated with the background. Second, the Boolean image is labeled to identify each set of connected nonzero pixels (they are the candidate particle images). Finally the area of these sets is matched against a maximum and a minimum admissible value in order to accept them as representative of particles and their positions are computed and stored together with temporal information for the succeeding trajectory recognition.

Trajectories are thus identified as time ordered series of particle locations that meet two criteria corresponding, respectively, to the assumption of maximum velocity and maximum acceleration in the flow field. These tracking parameters have been chosen according to the kinematic characteristics of each investigated field. This last procedure implies an interpolation of data over a regular grid and a consequent replacement of erroneous vectors with values computed starting from the neighboring vectors. Eulerian instantaneous velocity fields can then be obtained. Although PTV allows for the evaluation of velocity vectors with high local accuracy and assures a statistical independence of data,

Downloaded 17 May 2001 to 192.167.149.117. Redistribution subject to AIP license or copyright, see http://ojps.aip.org/phf/phfcr.jsp

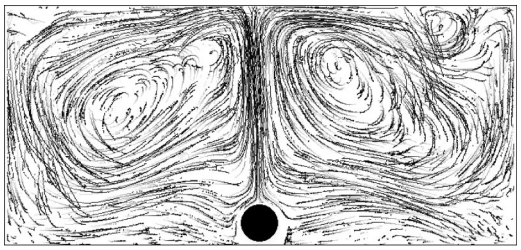

FIG. 2. An example of trajectories recognized by the PTV technique for the run at $\mathrm{Ra}=2.39\times10^{8}$. The trajectories are followed during 100 frames of their evolution. The circle on the bottom represents the linear heat source.

this procedure of interpolation should be carefully carried out in order to avoid errors.[18]

In Fig. 2 we show an example of trajectories recognized during 100 frames. From the above figure it is possible to see the two main counter-rotating vortices separated by the oscillating plume.

The Eulerian features of the flow have been investigated in details in a previous study.[14] In Fig. 3 we plot the horizontal component of the velocity obtained by an interpolation of PTV measurements in the middle of the cell. The time periodicity corresponding to the oscillation of the thermal plume is easily observed. In Fig. 4 we plot the power spectrum, which confirms the existence of a dominant periodic component in the velocity field.

In each run, the heat exchangers on the horizontal surfaces and the electrical resistance of the heater are activated about 3 h before the beginning of acquisition to avoid transient regimes. Acquisitions last for 2700 s, during this period 22 500 frames are digitized. Typically 900 particles are simultaneously tracked for each frame. Experiments have been performed for six different values of the heat flux supplied through the linear source. The values of the physical parameters for the runs are reported in Table I.

III. FINITE SIZE LAGRANGIAN LYAPUNOV ANALYSIS

The importance of chaotic advection in the transport of Lagrangian impurities is now well recognized.[5] This term refers to complex (turbulent-like) Lagrangian trajectories appearing in smooth, laminar, Eulerian flow. By definition, chaotic Lagrangian trajectories display sensitivity to initial conditions, i.e., the separation between two close trajectories diverges exponentially in time. The measure of the chaoticity of the motion is given by the (Lagrangian) Lyapunov exponent,[6] which represents the average rate of exponential divergence of two nearby trajectories.

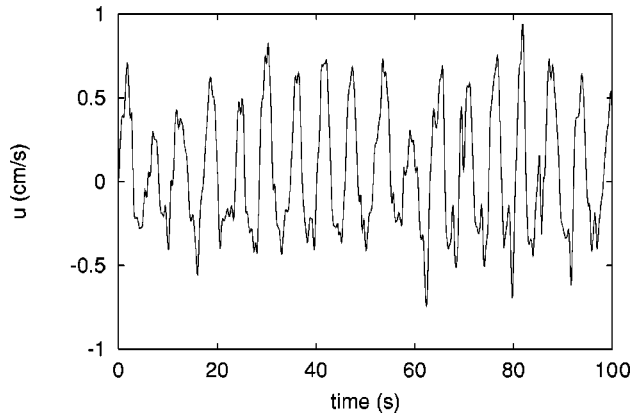

FIG. 3. Time series of Eulerian horizontal velocity obtained by interpolation of PTV velocities. The velocity is computed in a point above the heating element at a distance of $0.8H$ from the bottom.

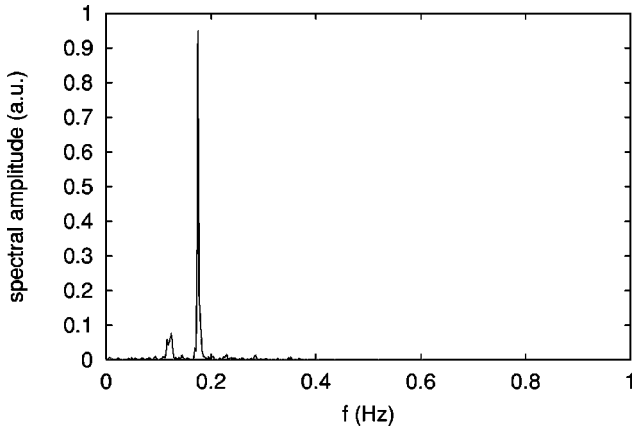

FIG. 4. Power spectrum of the horizontal velocity time series of Fig. 3. The main peak at frequency $f=0.175$ Hz corresponds to the thermal plume oscillations.

Suppose that $\mathbf{x}_1(t)$ and $\mathbf{x}_2(t)=\mathbf{x}_1(t)+\mathbf{R}(t)$ are two trajectories starting at $t=0$ at the distance $R_0=|\mathbf{R}(0)|$. The Lagrangian Lyapunov exponent is defined by

$$\lambda=\lim_{t\to\infty}\lim_{R(0)\to0}\frac{1}{t}\ln\frac{R(t)}{R(0)}, \tag{1}$$

where the inner limit is necessary in order to keep the separation $R(t)$ infinitesimal.

However, in practical (numerical or, even worse, experimental) computation of (1) one cannot attain the two limits. In numerical computation, the first limit $(t\to\infty)$ is replaced by a sufficiently long integration at which one observes the convergence of the Lyapunov exponent. The second limit $[R(0)\to0]$ can be handled[19] by periodically rescaling the separation vector $\mathbf{R}(t)$ in order to keep its modulus very small. Of course, if the first procedure can be very difficult, the latter is impossible in the case of experimental data. It is worth mentioning the rather powerful method to compute the Lyapunov exponent from time series introduced Wolf *et al.*[20]

Recently, a generalization of the Lyapunov exponent to finite separations has been proposed, called the finite size Lyapunov exponent.[16] The physical idea stems from the consideration that the separation R between the trajectories represents the scale at which one observes the system. The limit $R\to0$ in (1) physically means that λ is related to the smallest structures present in the flow. Otherwise, by keeping R finite and by means of the FSLE, $\lambda(R)$ one is able to quantify the dispersion properties of the flow at different length scales. The FSLE analysis has been demonstrated to be very useful both in numerical simulations of dispersion in fully developed turbulence[21] and the drifters' data analysis in the Mediterranean basin.[22]

Downloaded 17 May 2001 to 192.167.149.117. Redistribution subject to AIP license or copyright, see http://ojps.aip.org/phf/phfcr.jsp

TABLE I. Parameters related to the analyzed runs. Q is the heat flux injected into the system, ν the kinematic viscosity, κ the thermal diffusivity, and α the thermal dilatation factor.

Q(W/m)	$\nu(10^{-7}$ m^2/s)	$\kappa(10^{-7}$ m^2/s)	$\alpha(10^{-4}$ m^3/K)	Ra	Pr
1.00	8.850	1.441	2.593	6.87×10^7	6.14
3.50	8.870	1.440	2.583	2.39×10^8	6.16
8.25	8.720	1.444	2.652	5.96×10^8	6.04
12.20	9.440	1.429	2.329	7.20×10^8	6.61
22.4	8.380	1.452	2.815	1.74×10^9	5.77
29.20	8.560	1.447	2.729	2.17×10^9	5.92

The FSLE computation is based on the concept of separation doubling time, i.e., the time $T(R)$ it takes for the separation to grow from R to ρR, ρ being a constant larger than 1. The term ''doubling time'' refers properly only to the case $\rho=2$ (see the Appendix for a detailed description of the method). By performing a large number of doubling-time experiments, one defines the FSLE as (see Ref. 16)

$$\lambda(R)=\frac{1}{\langle T(R)\rangle_{\mathrm{e}}}\ln r, \tag{2}$$

where $\langle(\,)\rangle_{\mathrm{E}}$ is the average over many doubling-time experiments. The FSLE analysis looks very natural for the Lagrangian data of the present experiment. By means of the particle tracking algorithm one selects, frame by frame, nearby particles, say at separation R, and follows them measuring the time $T(R)$ it takes for the separation to growth up to ρR.

The finite size Lyapunov exponent at different R gives information concerning the different mechanisms of the spreading at different scales.[17] Let us clarify this point. If we assume to compute the FSLE for passive particles in a bounded domain (e.g., the vessel in our experiment) of typical size L_D advected by a flow of characteristic Eulerian scale $l_{\mathrm{E}}\ll L_D$, we expect for $\lambda(R)$ the following scale-dependent scenario.

(i) For small separation, $R\ll l_{\mathrm{E}}$, if the Lagrangian dynamics is chaotic, we recover the standard Lagrangian Lyapunov exponent. Indeed it is easy to show (see Ref. 16) that the following limit holds:

$$\lim_{R\to 0}\lambda(R)=\lambda. \tag{3}$$

(ii) If $l_{\mathrm{E}}\ll L_D$, in the intermediate regime $l_{\mathrm{E}}<R<L_D$, one can reasonably assume the two particles to be advected by almost uncorrelated velocities and, as a consequence, a diffusive behavior is expected, i.e., $\langle R^2(t)\rangle\simeq 4Dt$, where D is the diffusion coefficient. For the FSLE this means the scaling behavior

$$\lambda(R)\sim\frac{D}{R^2}. \tag{4}$$

(iii) At very large separation, $R\simeq L_D$, $\lambda(R)$ should go to zero because particles cannot separate more than the vessel size. Let us denote by $R_{\max}=O(L_D)$ the saturation value of R at the boundary. It has been shown[17] that in a large class of systems when R is close to $R_{\max}$, $\lambda(R)$ follows the universal behavior

$$\lambda(R)\simeq\frac{1}{\tau_R}\frac{R_{\max}-R}{R}, \tag{5}$$

where τ_R is the characteristic time of relaxation to the asymptotic uniform distribution (see the Appendix for more details).

For the convective flow studied in this paper, the Eulerian characteristic scale l_{E} is of the same order of the vessel dimension. Therefore, the diffusive regime (4) has no room to develop and we expect for the FLSE only the chaotic (3) and the saturation (5) regimes. The crossover between these regimes occurs at scales of the order of the Eulerian characteristic length scale associated with the convective pattern. Summarizing, from the finite size Lyapunov exponent analysis we can extract much information on the dispersion processes: the Lagrangian Lyapunov exponent (quantifying mixing time scale at small scale), the relaxation time τ_R for reaching uniform distribution at large scale, and an estimation of the Eulerian characteristic scale from Lagrangian measurements.

Let us conclude this section by observing that the FSLE analysis is an alternative to the relative dispersion analysis. Relative dispersion, i.e., the evolution of the separation of a couple of particles, is driven by the local velocity difference and thus gives information on the structure of the velocity field. The generic moment of relative dispersion is

$$\langle R(t)^p\rangle=\langle|\mathbf{x}_2(t)-\mathbf{x}_1(t)|^p\rangle, \tag{6}$$

where the average is taken over a large number of pairs. In the case of Lagrangian chaos one expects that for a small value of separation the relative dispersion grows exponentially with the Lyapunov exponent: $\langle R(t)\rangle\simeq R(0)\exp(\lambda t)$—this behavior is strictly verified only in the absence of intermittency and in the infinite time limit.[23]

At variance with the relative dispersion which computes the average separation at *fixed time*, the FSLE analysis computes the average doubling time at *fixed scale*. The general advantage is that the separation scale may be of dynamical relevance (i.e., one observes different diffusive properties at a different scale as discussed previously), while the standard average at fixed time may give rise to spurious contributions due to the superposition of realizations which attain different scales at the same time (see the examples in Ref. 17). In the case of the present experimental data, we will see in Sec. IV that the analysis in terms of relative dispersion (6) indeed gives little information.

Downloaded 17 May 2001 to 192.167.149.117. Redistribution subject to AIP license or copyright, see http://ojps.aip.org/phf/phfcr.jsp

IV. DATA ANALYSIS

A. Finite size Lyapunov exponent from Lagrangian data

The convective pattern realized in our experiment is essentially a two-dimensional, time-dependent flow even at very high Rayleigh numbers. Therefore, as discussed in Sec. I, we expect chaotic Lagrangian motion.[5,6] We used the FSLE analysis for the experimental trajectories in order to probe the separation growth at different scales from the Lyapunov exponential regime up to the saturation regime (5). For all the results presented in the following we use as unit length the height of the cell, H, and as unit time the diffusive time $t_\kappa = H^2/\kappa \simeq 2.5\times 10^4$ s.

We report the results for six runs at different Rayleigh numbers (see Table I). Each run consists of 22 500 frames with 900 trajectories on average. None of the trajectories lasts for the whole run for two reasons. The first refers to a failure of the tracking algorithm in following particles very close to boundaries and to the heat source because of light reflections. The second refers to particles which are lost because of the nonperfect two-dimensional nature of the flow. Nevertheless, we find a large number of trajectories that last for some circulation time.

The FSLE analysis on the experimental data has been done as follows. We fixed a set of thresholds $R_n = R_0\rho^n$ ($n = 0,\ldots,N$), each time t_0 a new couple was considered whenever two particles (not yet forming a couple) were at a distance $R(t_0) \leqslant R_0$. The separation growth between these particles is then followed for times $t > t_0$ and the ''doubling times,'' $T_\rho(R_n)$, at scale R_n are evaluated by measuring the time the separation takes to grow from R_n up to $R_{n+1} = \rho R_n$. Since trajectories are sampled at discrete times, the average over for computing $\lambda(R)$ is done following (A4), which extends (2) to the time-discrete case (see the Appendix).

In order to increase the statistics at large separations R, we computed the FSLE for different values of the smallest scale R_0 ($R_0 = 0.067\,H$, $0.1\,H$, $0.13\,H$). The threshold rate ρ is set equal to 1.2 in each computation.

Figure 5 shows the FSLE computed for two different Rayleigh numbers ($\mathrm{Ra} = 2.39\times 10^8$ and $\mathrm{Ra} = 5.96\times 10^8$). We observe the collapse of $\lambda(R)$ to the plateau of the Lyapunov exponent λ at small values of R. Since we find $\lambda > 0$, we have direct evidence of Lagrangian chaos in the investigated flow.[24]

For larger separation $\lambda(R)$ drops to smaller values, indicating a slowing down in the separation growth. This is quantitatively well described by the saturation regime (5). The collapse of the curves at different R_0 confirms that sufficiently high statistics is reached even at large scales. Fluctuation among different R_0 curves can be taken as an estimation of the error for $\lambda(R)$.

From the general discussion of Sec. III, we expect that the crossover from the exponential regime gives an estimation of the characteristic Eulerian scale l_E. We find $l_\mathrm{E} \simeq 0.5$ H, which is indeed close to what one could expect from Fig. 2. Because the Eulerian scale is close to the saturation value, $l_\mathrm{E} \simeq L_D$, we do not expect to observe the intermediate diffusive regime.

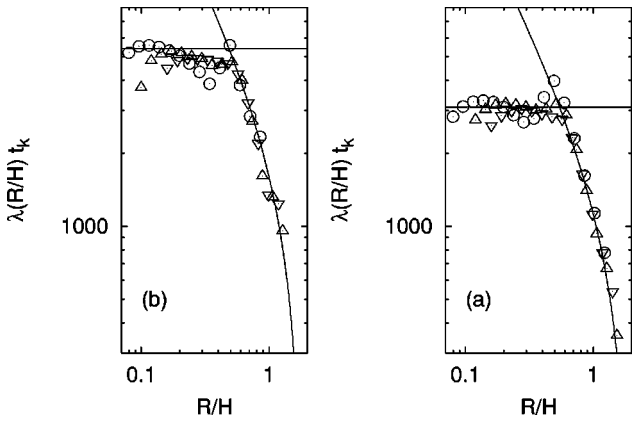

FIG. 5. (a) $\lambda(R)$ vs R for different initial thresholds $R_0 = 0.067$ H, 0.1 H, 0.13 H at $\mathrm{Ra} = 2.39\times 10^8$. The horizontal line is the Lyapunov exponent $\lambda = 3100 \pm 2001/t_\kappa$; the curve is the saturation regime (5) with $\tau_R = 8.0\times 10^{-4}\, t_\kappa$ and $R_{\max} = 1.9\,H$. (b) The same as in (a) for $\mathrm{Ra} = 5.96\times 10^8$. Here $\lambda = 5400 \pm 6001/t_\kappa$, $\tau_R = 5.0\times 10^{-4}\, t_\kappa$, and $R_{\max} = 1.8$ H.

The fit of Fig. 5 with the saturation regime (5) allows us to estimate the saturation scale $R_{\max} \simeq 1.9\,H$ and the relaxation time $\tau_R \simeq 8.0\times 10^{-4} t_\kappa$. We observe that both $1/\lambda$ (an estimation of the small scale mixing time) and τ_R are much smaller than the diffusive time t_κ. This means that dispersion of Lagrangian tracers in the convective cell is dominated by chaotic advection. In addition, we observe that the characteristic scales l_E and $R_{\max}$ seem to be independent of the Rayleigh number.

Let us conclude this section by comparing the FSLE and the relative dispersion analysis. For the same trajectories of Fig. 5(a) we have computed the moments of relative dispersion (6). The result, plotted in Fig. 6, deserves some comments. At small times (i.e., small separation) an exponential regime is indeed observed, but with a slope which increases with the moment p. The reason for this behavior is that many pairs remain very close while advected in the convective cell for very long times before the exponential separation takes

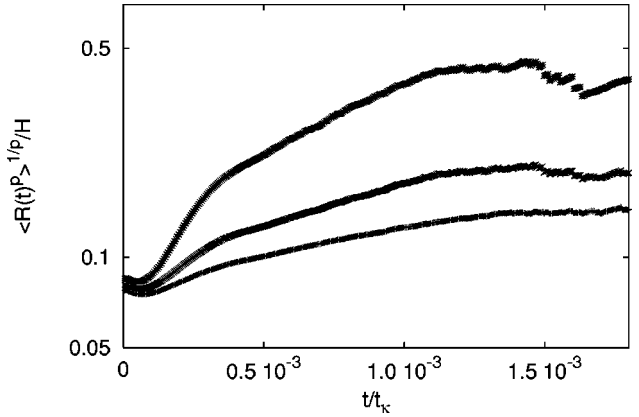

FIG. 6. Rescaled relative dispersion $\langle R(t)^p\rangle^{(1/p)}$ for $p = 1,2,4$ (from bottom to top) in lin–log plot. The dependence of the slope on the order p is an indication of the strong intermittency in the Lagrangian separation.

Downloaded 17 May 2001 to 192.167.149.117. Redistribution subject to AIP license or copyright, see http://ojps.aip.org/phf/phfcr.jsp

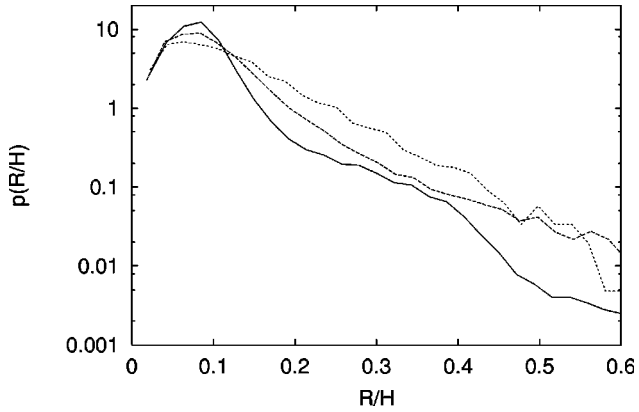

FIG. 7. Probability distribution function of pair separations at times $t=2.5\times10^{-4}\,t_\kappa$ (full line), $t=5.0\times10^{-4}t_\kappa$ (dashed line), and $t=1.0\times10^{-3}\,t_\kappa$ (dotted line) in lin–log plot.

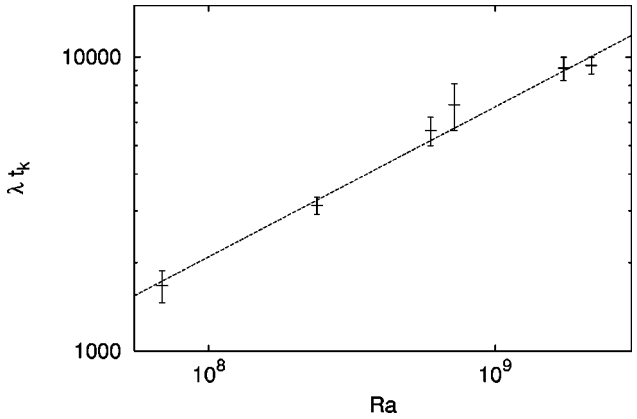

FIG. 8. Lagrangian Lyapunov exponent as a function of Ra. The errors are estimated by the fluctuations at different initial R_0. The line is the best fit $\lambda\sim \mathrm{Ra}^{0.51}$.

place. As a confirmation of this picture, in Fig. 7 we plot the probability distribution function of the pair distance for different times: The tail of the distribution is representative of the particles which effectively separate. As is clearly shown in Fig. 7, the evolution of the distribution is not self-similar in time and most of the couples (the peak of the distribution) remain close for a long time. Moreover, at large times and distances, a second problem appears. Indeed, for times longer than the circulation time, some of the separated particles come close again, causing strong fluctuations in the relative dispersion (see Fig. 6). As a consequence, the saturation regime analogous to (5) is not observable with this kind of analysis.

Neither of these problems affect the FSLE analysis which performs the statistics only on the pairs which separate. The statistics are thus not affected by particles trapped in the nonchaotic vortex core, a feature which is generally observed in presence of vortices in two-dimensional flows.[25] The comparison of Figs. 5 and 6, obtained from the same set of trajectories, is a convincing demonstration of the advantage of fixed scale analysis with respect to the fixed time one.

B. Dependence of the Lagrangian quantities on the Rayleigh number

In order to explore the dependence of the Lagrangian statistics on the Eulerian characteristics, we have performed the FSLE analysis for a Rayleigh number which varies over more than one order of magnitude (see Table I). The dependence of the Lagrangian Lyapunov exponent on Ra is shown in Fig. 8. A clear scaling is observed, indicating a power law dependence

$$\lambda\sim \mathrm{Ra}^{\gamma} \tag{7}$$

with $\gamma=0.51\pm0.02$. An analogous scaling has been observed for the Eulerian characteristic times in a similar flow.[14]

On the basis of the above-mentioned result and taking into account the independence of l_E and $R_{\max}$ of the Rayleigh number, we compensate $\lambda(R)$ at different Ra with $\mathrm{Ra}^{1/2}$, according to the scaling (7). The result is plotted in Fig. 9. We observe a fairly good collapse at all the length scales, the saturation regime (5) included, the fluctuations are of the order of the error reported in Fig. 5.

The conjecture that $\lambda(R)/\mathrm{Ra}^{1/2}$ is a Rayleigh independent function can be supported by the following dimensional argument. The equations of motion in the Boussinesq approximation and made nondimensional by using H as the unit length, the diffusive time t_κ as unit time, and rescaling the temperature fluctuations with the typical temperature difference ΔT are given by[13]

$$\frac{1}{\mathrm{Pr}}\left[\frac{\partial u_\alpha}{\partial t}+u_\beta\frac{\partial u_\alpha}{\partial x_\beta}+\frac{\partial}{\partial x_\alpha}p\right]=\frac{\partial^2 u_\alpha}{\partial x^2}-\mathrm{Ra}\,T z_\alpha, \tag{8}$$

$$\frac{\partial T}{\partial t}+u_\beta\frac{\partial T}{\partial x_\beta}=\frac{\partial^2 T}{\partial x^2}. \tag{9}$$

It is easy to verify this performing the following rescaling:

$$u_\alpha\to\Lambda u_\alpha,\quad t\to\Lambda^{-1}t,\quad \mathrm{Ra}\to\Lambda^2\,\mathrm{Ra}, \tag{10}$$

where Λ is an arbitrary factor, Eqs. (8) and (9) remain unchanged, if one disregards the diffusive terms. This means that, neglecting the diffusive terms, the Boussinesq equations at fixed Pr (as in our experiment, see Table I) are invariant under the rescaling (10). As a further argument in favor of

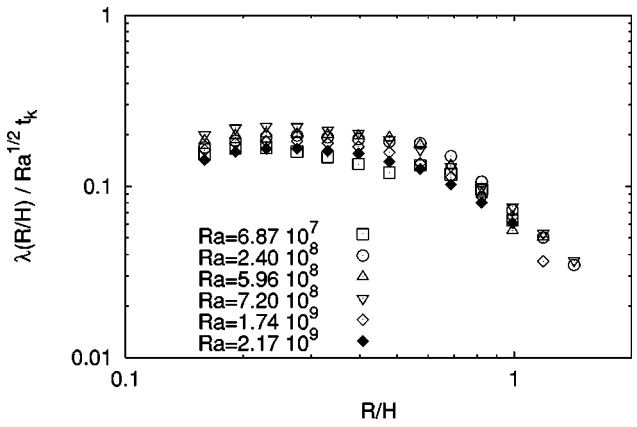

FIG. 9. Data collapse of $\lambda(R)$ at different Ra rescaled with $\mathrm{Ra}^{1/2}$.

Downloaded 17 May 2001 to 192.167.149.117. Redistribution subject to AIP license or copyright, see http://ojps.aip.org/phf/phfcr.jsp

neglecting the diffusive terms and thus in favor of the scaling invariance, let us observe that the large values of the Lyapunov exponent in units of diffusion time give a strong indication of Lagrangian dispersion ruled by chaotic advection.

The consequence of the Eulerian scaling invariance on the Lagrangian motion, given by

$$\frac{d\mathbf{x}(\mathbf{t})}{dt}=\mathbf{u}(\mathbf{x}(\mathbf{t}),t), \tag{11}$$

is that Lagrangian trajectories are independent of the Rayleigh number. Therefore, the FSLE exponent, which is dimensionally an inverse time, scales as $\mathrm{Ra}^{1/2}$, which is (7).

Of course, for the scaling invariance (10) to be observable, the stability of the flow is required. For large enough Ra (above the values investigated in this paper) we would observe the transition to different Eulerian regimes and thus a deviation from the scaling relation (7).

V. CONCLUSIONS

The relative dispersion of Lagrangian tracers in a convective flow confined in a vessel is studied at different Rayleigh numbers. The particle velocimetry tracking technique is used to obtain a large number of Lagrangian trajectories. Dispersion properties have been quantified by using the recently introduced finite size Lyapunov exponent, which measures the dispersion growth rate at different scales (i.e., at different distances between particles). In the limiting cases in which there is a large scale separation between the Eulerian characteristic length scale and the domain size, the FSLE analysis and the usual way of looking at the relative dispersion at fixed delay times give the same information. In our experiment, where the vessel size is not much larger than the Eulerian length, the customary relative dispersion analysis is affected by problems due to the lack of an asymptotic regime. Therefore, the FSLE analysis turns out to be more suitable in investigating the dispersion properties.

At small scale the FSLE gives the Lagrangian Lyapunov exponent $[\lambda(R)=\lambda]$, which is found to be positive. This means that small scale mixing is driven by chaotic advection. At large scale the FSLE behavior is well described by a general law which takes into account the presence of boundaries.

We have also observed that the degree of chaoticity depends on the Rayleigh number. In particular, the Lagrangian Lyapunov exponent displays a power law dependence on the Rayleigh number, i.e., $\lambda \sim \mathrm{Ra}^{1/2}$. Moreover, the FSLE displays the same $\mathrm{Ra}^{1/2}$ dependence also at large scales. Indeed after a suitable rescaling, the FSLE curves measured at different Rayleigh numbers collapse on the same curve. The power law behavior and the collapse of the FSLE curves on the whole range of scales are explained on the grounds of the scaling invariance of the Boussinesq equation. This invariance requires one to neglect diffusive terms, meaning that diffusion plays a marginal role for the Lagrangian dynamics, as confirmed by the high value of the Lagrangian Lyapunov exponent measured in units of diffusive time.

ACKNOWLEDGMENTS

We thank A. Celani, A. Cenedese, S. Ciliberto, J. F. Pinton, G. P. Romano, and A. Vulpiani for useful discussions. In particular, we thank M. Tardia for his contributions during the data acquisition.

This work is partially supported by INFM (Progetto Ricerca Avanzata TURBO) and by MURST (Contract No. 9908264583)

APPENDIX: COMPUTATION OF THE FINITE SIZE LYAPUNOV EXPONENT

Here we describe the method employed for the computation of the finite size Lyapunov exponent. We also discuss a simple argument for the asymptotic formula (5), which describes the behavior near saturation.

The practical method for the FSLE computation goes as follows. One has to choose a norm to evaluate the distance $R(t)$ between two trajectories and to define a series of thresholds $R_n=\rho^n R_0$ $(n=1,\ldots,N)$. Then one measures the ''doubling times'' $T_\rho(R_n)$ that a separation of size R_n takes to grow up to R_{n+1}. The threshold rate ρ should not be fixed too large in order to avoid the separation growth through different scales before reaching the next threshold and the possible mixing of effects belonging to different scales. On the other hand, ρ cannot be too close to one, otherwise $T_\rho(R)$ tends to be of the order of the time step (numerical integration) or of the sampling time (experimental data analysis). For simplicity we call T_ρ ''doubling time'' even if $\rho \neq 2$.

For computing the doubling times, one has usually to follow two trajectories starting at an initial $R_{\min} \ll R_0$, in order to permit the initial perturbation to align with the most unstable direction in the phase space. Moreover, one must pay attention to keep $R_N < R_{\max}$, $R_{\max}$ being the saturation distance, so that all the thresholds can be attained.

The evolution of the separation from its initial value $R_{\min}$ to the largest threshold R_N carries out a single separation growth experiment during which one measures a realization of all the $T_\rho(R_n)$. When the largest threshold is reached one considers a new couple of trajectories obtained by rescaling the separation to the initial distance $R_{\min}$ and starts another experiment. In the case of experimental data, one searches at each time for close particles and follows their separation evolution.

After $\mathcal{N}$ experiments, the expectation value of a quantity A is evaluated as

$$\langle A\rangle_e=\frac{1}{\mathcal{N}}\sum_{i=1}^{\mathcal{N}} A_i, \tag{A1}$$

where $\langle(\,)\rangle_e$ indicates the average over many realizations of the pair's separation evolution, which is not the same as the time average because different separation growth experiments may take different times. The connection between the time average and the average (A1) is given by

$$\langle A\rangle_t=\frac{1}{T}\int_0^T A(t)\,dt=\frac{\Sigma_i A_i \tau_i}{\Sigma_i \tau_i}=\frac{\langle A\tau\rangle_e}{\langle \tau\rangle_e}. \tag{A2}$$

Downloaded 17 May 2001 to 192.167.149.117. Redistribution subject to AIP license or copyright, see http://ojps.aip.org/phf/phfcr.jsp

To compute the Lyapunov exponent one has to evaluate $\langle 1/T_\rho(R)\rangle_t$, i.e., the inverse of doubling time itself, therefore, from Eq. (A2) with $A=1/T_\rho(R_n)$ one recovers Eq. (2), i.e.,

$$\lambda(R_n)=\frac{1}{\langle T_\rho(R_n)\rangle_e}\ln\rho. \tag{A3}$$

The above-described method needs the distance between the two trajectories to be continuous in time. This is not true for maps and for experimental data (i.e., discrete sampling in time). In these cases the method has to be slightly modified. Now, $T_\rho(R_n)$ is defined as the minimum time such that $R(T_\rho(R_n))\geqslant\rho R_n$, and $R(T_\rho)$ becomes a fluctuating quantity, then from (A2) one has

$$\lambda(R_n)=\frac{1}{\langle T_\rho(R_n)\rangle_e}\left\langle \ln\left(\frac{R(T_\rho)}{R_n}\right)\right\rangle_e. \tag{A4}$$

Now we discuss the derivation of Eq. (5), i.e., the behavior of $\lambda(R)$ near the saturation. This behavior mainly stems from the assumption that after large time intervals, the tracers tend to uniformly distribute in the domain (e.g., the vessel) and that small deviations from the asymptotic uniform distribution relax exponentially to that. This assumption is usually satisfied in generic dynamical systems even if it is difficult to prove. In the language of chaotic dynamical systems, exponential relaxation to asymptotic distribution means that the second eigenvalue α of the Perron–Frobenius operator is inside the unitary circle and the relaxation time is $\tau_R=-\ln|\alpha|$. [26]

If the distribution relaxes exponentially to the uniform one, the same is expected to hold also for the moments of the distribution. Therefore, for the large time evolution of the separation one expects:

$$\langle R(t)\rangle_s\approx R_{\max}-\tilde{R}e^{-t/\tau_R}, \tag{A5}$$

where $\tilde{R}$ and τ_R depend on the system, and $\langle[\ ]\rangle_s$ denotes the spatial average on the probability distribution. For $t\ll\tau_R$ or equivalently for $(R_{\max}-\langle R(t)\rangle_s)/\langle R(t)\rangle_s\ll 1$, we expect

$$\frac{d}{dt}\ln\langle R(t)\rangle_s=\lambda(R)=\frac{1}{\tau_R}\frac{R_{\max}-R}{R}, \tag{A6}$$

which is Eq. (5). For an exact computation of Eqs. (A5)–(A6) in a particular system see the Appendix in Ref. 17.

[1] H. K. Moffat, ''Transport effects associated with turbulence with particular attention to the influence of helicity,'' Rep. Prog. Phys. **46**, 621 (1983).
[2] A. Monin and A. Yaglom, *Statistical Fluid Dynamics* (MIT, Cambridge, 1983).
[3] G. I. Taylor, ''Diffusion by continuous movements,'' Proc. London Math. Soc. **20**, 196 (1921).
[4] H. Aref, ''Integrable, chaotic, and turbulent vortex motions in two dimensional flows,'' Annu. Rev. Fluid Mech. **15**, 345 (1983); ''Stirring by chaotic advection,'' J. Fluid Mech. **143**, 1 (1984).
[5] J. M Ottino, *The Kinematics of Mixing: Stretching, Chaos and Transport* (Cambridge University Press, Cambridge, 1989).
[6] A. Crisanti, M. Falcioni, G. Paladin, and A. Vulpiani, ''Lagrangian chaos: Transport, mixing and diffusion in fluids,'' Riv. Nuovo Cimento **14**, 1 (1991).
[7] T. H. Solomon and J. P. Gollub, ''Chaotic particle transport in time-dependent Rayleigh–Bénard convection,'' Phys. Rev. A **38**, 6280 (1988).
[8] J. P. Gollub and T. H. Solomon, ''Complex particles trajectories and transport in stationary and periodic convective flows,'' Phys. Scr. **40**, 430 (1989).
[9] T. H. Solomon, E. R. Weeks, and H. L. Swinney, ''Chaotic advection in two-dimensional flow: Lèvy flights and anomalous diffusion,'' Physica D **76**, 70 (1994).
[10] J. Gugkenheimer and P. Holmes, *Nonlinear Oscillations, Dynamical Systems, and Bifurcations of Vector Fields* (Springer, Berlin, 1986).
[11] T. M. Antonsen, Jr., Z. Fan, E. Ott, and E. Garcia-Lopez, ''The role of chaotic orbits in the determination of power spectra of passive scalars,'' Phys. Fluids **8**, 3094 (1996).
[12] G. Desrayaud and G. Lauriat, ''Unsteady confined buoyant plumes,'' J. Fluid Mech. **252**, 617 (1993).
[13] L. D. Landau and E. M. Lifshiz, *Fluid Mechanics*, 2nd ed. (Pergamon, Oxford, 1987).
[14] M. Miozzi, G. Querzoli, and G. P. Romano, ''The investigation of an unstable convective flow using optical methods,'' Phys. Fluids **10**, 2995 (1998).
[15] G. Querzoli, ''A Lagrangian study of particle dispersion in the unstable boundary layer,'' Atmos. Environ. **16**, 2821 (1996).
[16] E. Aurell, G. Boffetta, A. Crisanti, G. Paladin, and A. Vulpiani, ''Growth of noninfinitesimal perturbations in turbulence,'' Phys. Rev. Lett. **77**, 1262 (1996); ''Predictability in the large: An extension of the concept of Lyapunov exponent,'' J. Phys. A **30**, 1 (1997).
[17] V. Artale, G. Boffetta, A. Celani, M. Cencini, and A. Vulpiani, ''Dispersion of passive tracers in closed basins: Beyond the diffusion coefficient,'' Phys. Fluids **9**, 3162 (1997).
[18] R. J. Adrian, ''Particle-imaging techniques for experimental fluid mechanics,'' Annu. Rev. Fluid Mech. **23**, 261 (1991).
[19] G. Benettin, L. Galgani, A. Giorgilli, and J. M. Strelcyn, ''Lyapunov characteristic exponents for smooth dynamical systems and for Hamiltonian systems: A method for computing all of them,'' Meccanica **15**, 9 (1980).
[20] A. Wolf, J. B. Swift, H. L. Swinney, and J. A. Vastano, ''Determining Lyapunov exponents from a time series,'' Physica D **16**, 285 (1985).
[21] G. Boffetta, A. Celani, A. Crisanti, and A. Vulpiani, ''Relative dispersion in fully developed turbulence: Lagrangian statistics in synthetic flows,'' Europhys. Lett. **42**, 177 (1999).
[22] G. Lacorata, E. Aurell, and A. Vulpiani, ''Relative dispersion in the Adriatic Sea: Lagrangian data and chaotic model,'' preprint, chao-dyn/9902014 (1999).
[23] T. Bohr, M. H. Jensen, G. Paladin, and A. Vulpiani, *Dynamical Systems Approach to Turbulence* (Cambridge University Press, Cambridge, 1998).
[24] G. Boffetta, M. Cencini, S. Espa, and G. Querzoli, ''Experimental evidence of chaotic advection in a convective flow'' Europhys. Lett. **48**, 629 (1999).
[25] A. Babiano, G. Boffetta, A. Provenzale, and A. Vulpiani, ''Chaotic advection in point vortex models and two-dimensional turbulence,'' Phys. Fluids **6**, 2465 (1994).
[26] E. Ott, *Chaos in Dynamical Systems* (Cambridge University Press, Cambridge, 1993).

Downloaded 17 May 2001 to 192.167.149.117. Redistribution subject to AIP license or copyright, see http://ojps.aip.org/phf/phfcr.jsp